Particle & Particle Systems Characterization

www.particle-journal.com

Giant Exchange-Bias in Polyol-Made $CoFe_2O_4$-CoO Core–Shell Like Nanoparticles

Nancy Flores-Martinez, Giulia Franceschin, Thomas Gaudisson, Patricia Beaunier, Nader Yaacoub, Jean-Marc Grenèche, Raul Valenzuela, and Souad Ammar**

Cobalt ferrite ferrimagnetic nanoparticles (NPs) are prepared and used in this work as seeds to grow a thin antiferromagnetic poly- and nanocrystalline CoO shell. The major purpose is to study systematically the characteristics of the as-produced powders, making emphasis on their internal crystallographic arrangement and their magnetic properties. ^{57}Fe Mössbauer spectrometry evidences an evolution of the cation distribution among the spinel lattice in the cobalt ferrite core during the core–shell NPs processing. High-resolution transmission electron microscopy shows a perfect epitaxy between the face-centered cubic lattices of the spinel core and the rock-salt shell. Finally, the measurements of 7T-field-cooled magnetic hysteresis loops at low temperature (5 K) of the composite particles exhibit a strong exchange bias coupling with an exchange field, $\mu_0 H_E$, of 365 mT and an enhanced coercive field, $\mu_0 H_C$, of 1395 mT. These values are very high compared to those of differently prepared CoO-based oxide composite NPs and for which a giant exchange-bias is reported. These features are attributed to the favorable material processing conditions offered by the polyol process in terms of crystalline quality, particularly at the interfaces, and for the pinning action exerted by the CoO phase on the magnetization of the $CoFe_2O_4$ phase.

Dr. N. Flores-Martinez, Dr. G. Franceschin, Dr. T. Gaudisson, Prof. S. Ammar
Université Paris Diderot
Sorbonne Paris Cité
CNRS UMR-7086
ITODYS
15 Rue Jean-Antoine de Baïf, 75251 Paris, France
E-mail: nancy.flores@univ-paris-diderot.fr; ammarmer@univ-paris-diderot.fr

Dr. P. Beaunier
Sorbonne Université
CNRS UMR-7197
LRS
4 Place Jussieu, 75005 Paris, France

Dr. N. Yaacoub, Dr. J.-M. Grenèche
Université du Maine
CNRS UMR-6283
IMMM
Avenue Olivier Messiaen, 72085 Le Mans, France

Prof. R. Valenzuela
IIM
Universidad Nacional Autónoma de México
Circuito Exterior S/N, Ciudad Universitaria
Coyoacán, 04510 CDMX, Mexico

The ORCID identification number(s) for the author(s) of this article can be found under https://doi.org/10.1002/ppsc.201800290.

DOI: 10.1002/ppsc.201800290

1. Introduction

The combination of a ferromagnetic or ferrimagnetic (F) material, with an antiferromagnetic (AF) material, can lead to a spin exchange coupling, at the interface, known as "exchange bias" (EB). EB was first discovered by Meiklejohn and Bean in 1956[1] in metallic Co particles with a surface oxidation to cobalt oxide (Co@CoO). It is usually characterized by an asymmetric hysteresis loop and an enhanced coercive field, H_C. This feature is the origin of several active applied researches, since it can be used for magnetic recording heads,[2,3] magnetoresistive random access memories (MRRAM),[4–6] permanent magnets,[7,8] and high-density granular magnetic recording media.[9,10] A number of excellent reviews on the subject have been published reporting EB in differently shaped nanomaterials: bilayer systems,[11] core–shell nanoparticles (NPs),[1,12,13] nanomagnets embedded in an AF matrix,[14] and spin-glass phases in nanostructures.[15,16] In addition, EB has been observed in a variety of ferromagnetic metals and ferrimagnetic oxides. Focusing on oxides, it was reported in double perovskites,[17] manganites,[18] cobaltites,[19] garnets,[20] hexaferrites,[21] and spinel ferrites.[22–24] For most of these systems, a shift and a broadening of the hysteresis loops were observed in magnetic field cooling operating conditions. As significant they are as the crystallographic coherence between the contacted F and AF phases, their good size proportion and their optimized weight ratio are achieved, making some authors calling certain oxide-based granular composites as "giant exchange bias" systems, like $SrFe_{12}O_{19}$@CoO[21] and $CoFe_2O_4$@Co_3O_4[24] ones. All these previous studies underline the importance of the chemical nature of the involved F and AF phases in EB onset. So, in this context the choise of spinel ferrites and rock-salt monoxides as F and AF components of core–shell hetero-nanostructures, thanks to the structural proximity, the chemical stability, and the tunability of the magnetic properties of these phases, offers the best opportunity to build robust exchange-biased systems. Besides, the synthesis process may also be crucial, since it can tailor the internal structure of the NPs, define their shape and size, and affect their interface quality. For instance, it was already reported that acting on the synthesis conditions of ferrite spinel core particles may change their local structure,

with a deviation of their crystallographic lattice from a thermodynamically stable one into a deviated one.[25–27] As a result, a decrease or an increase of the magnetocrystalline anisotropy constant, Curie temperature, saturation magnetization, and so on may occur, which is not totally inconsequential on EB. Similarly, possible cation interdiffusion during core@shell NPs production by seed mediated growth in a solution,[26,27] with an improvement of the interface arrangement (epitaxy) and then an enhancement of EB feature was reported.

In this context, considering a promising exchange-biased system, namely $CoFe_2O_4$@CoO, in which both F and AF phases exhibit a high magnetocrystalline anisotropy constant and relevant magnetic ordering temperatures, T_C = 850 K for bulk $CoFe_2O_4$ and T_N = 298 K for bulk CoO, we decided to produce such NPs by means of the polyol process, with a special emphasis on EB and the effect of the seed mediated growth processing on it.

2. Results and Discussion

2.1. Structural Properties

For commodity, cobalt ferrite and cobalt monoxide phases are named *CFO* and *CO*, respectively, hereafter.

First, the chemical composition of all the produced powders was checked by X-ray fluorescence (XRF) spectroscopy, focusing on the atomic ratio between Fe and Co elements. As expected, it was found to be consistent with i) the production of cobalt ferrite in the *CFO* powder and ii) the formation of a composite made from about 58 and 42 wt% of cobalt ferrite and cobalt monoxide, respectively, in the *CFO-CO* powder (**Table 1**).

Second, the crystalline structure was investigated by X-ray diffraction (XRD). The recorded patterns were compared (**Figure 1**) and were analyzed by Rietveld refinement using the well-known MAUD software.[28] The fitting procedure and result are detailed in Figure SI-1 in the Supporting Information. All the diffraction peaks of the seed powder belong to the spinel structure with a refined cell parameter in good agreement with the $CoFe_2O_4$ ICDD card reference n°98-010-9044. An increase of only 0.09% was measured between the reference cell parameter value and that refined here. Additional reflections are observed in the composite powder, matching all of them with the CoO structure (ICDD card reference n°98-000-9865) (**Table 2**). The refined weight content of the *CFO* and *CO* phases were found to be 60 and 40 wt% for unit cell parameters of a = 8.410(5) and 4.266(5) Å, respectively. The former values are close to those determined by XRF, in the limit of experimental errors, and the latter are also close to those tabulated for bulk $CoFe_2O_4$ and CoO, with an increase of less than 0.17% and 0.05%, respectively. This increase is not at all significant, considering the accuracy of the refined values, but it can reflect

Table 1. Main XRF results obtained on *CFO* and *CFO-CO* particles.

	Fe (at %) ±2	Co (at %) ±2	[*CFO*]/[*CFO*+*CO*] (wt%) ±2
CFO	67	33	100
CFO-CO	39	61	58

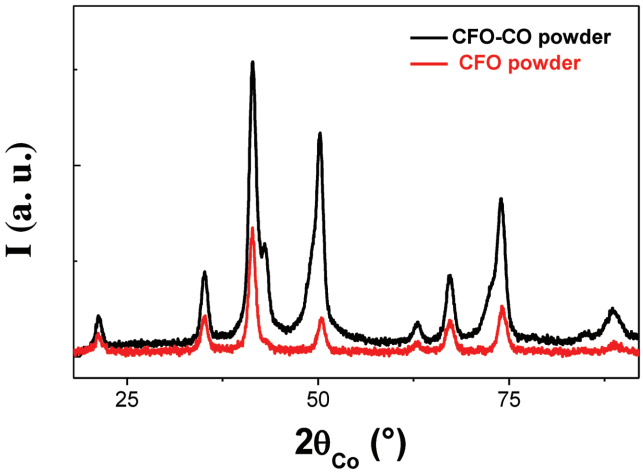

Figure 1. XRD pattern of *CFO-CO* composite powder (black line) compared to that of pure *CFO* (red line) Both samples were synthesized by the polyol process.

a weak structural evolution of the spinel phase by comparison to the seed powder. In this case, such an evolution may have drastic consequences on the magnetic properties of the F phase, since a deviation from the inverse spinel structure can be correlated to a decrease of the magnetocrystalline anisotropy energy.

Indeed, there is a basic correlation between the cell parameter value and the anion–cation distance for a particular site in the spinel structure, and thus between the cell parameter and the cation distribution among the tetrahedral (A) and octahedral (B) sites of a spinel lattice. A partial transfer of Co^{2+} cations from B into A sites, and reversely, a corresponding transfer of Fe^{3+} cations from A into B sites, must lead to a small increase of the lattice cell parameter,[29–31] but a significant decrease of the spin-orbit contribution on cobalt ions. Divalent cobalt cations being systematically larger than ferric ones,[29] a double cation transfer induces a decrease and an increase of the R_A and R_B values, which measure exactly the average value of the anion–cation distance on the A and B sites, respectively, and then an increase of the unit cell value.[32] Unfortunately, the atomic number proximity between Co and Fe atoms does not allow a correct refinement of the spinel site occupation ratio by each of them from the collected XRD data.

To tentatively elucidate a possible deviation of the spinel structure, ^{57}Fe Mössbauer spectra of the composite *CFO-CO* powder were recorded at 300 and 77 K and compared to those of the bare *CFO* one (**Figure 2**). Interestingly, at the two temperatures, there are no notable differences between the spectra of the two samples. Seed and composite powders have a spectrum at room temperature consistent with a broadened lines sextet. This means that the superparamagnetic relaxation effects on the ferrimagnetic spinel phase are less important at this temperature, but not yet vanished. The lack of resolution of the recorded spectra does not allow better fitting than that by means of a discrete hyperfine field distribution leading to the determination of average hyperfine parameter values (**Table 3**). A mean isomer shift $<\delta>$ of 0.33 mm s^{-1} and a mean hyperfine field $<B_h>$ of about 44 T were measured for the two samples, which are consistent with iron in the Fe^{3+} valence state mainly. They are also close to those usually observed on nanocrystalline

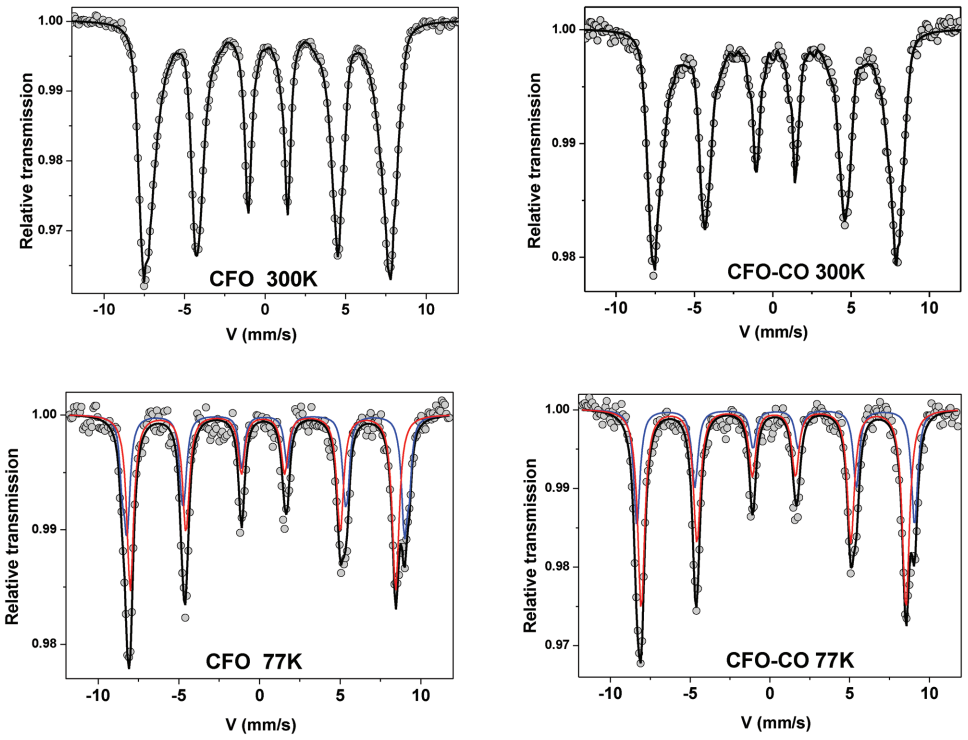

Figure 2. Mössbauer spectra recorded at 300 and 77 K on *CFO* and *CFO-CO* powders. The scatters and the continuous black line correspond to the experimental data and the total calculated ones, assuming two iron contributions, a ferric (red line) and a ferrous-type (blue line), respectively.

polyol-made cobalt ferrite particles at room temperature.[25] On the contrary, the Mössbauer spectra recorded at 77 K show different hyperfine structures with more resolved magnetic sextets (Figure 2). Indeed, each spectrum can be decomposed into two sextets composed of sharp Lorentzian lines and with isomer shifts δ of 0.51 ± 0.02 and 0.38 ± 0.02 mm s^{-1} and hyperfine fields of B_h 53.7 ± 0.5 and 50.8 ± 0.5 T: they correspond to Fe^{3+} ions in A and B spinel sites, respectively, and are close to the expected values for bulk[33] and nanocrystalline[25,32,34] cobalt ferrite. One does emphasize that the resolution of the present hyperfine structures does not require low-temperature in-field Mössbauer measurements which give rise to an accurate estimate of the proportions of the two components.[35] Assuming equal recoilless fraction Lamb–Mössbauer factors (f) for A and B Fe sites, the A/B population ratio is found to be 0.75 for the seed powder, far from the expected typical value of an exact inverse spinel cobalt ferrite (0.50). It is found to be 0.51 for the composite one. In other words, the structure of the spinel phase in the composite powder is closer to that of the thermodynamically stable cobalt ferrite than that of the spinel phase in the seed powder. This structural discrepancy is most probably due to the fact that the *CO* growth on *CFO* seeds, during composite powder synthesis, is performed within refluxing condition for a prolonged heating time (about 18 h). Such a long heating provides enough energy to the system to allow the migration of a certain number of Co^{2+} cations from the tetrahedral to the octahedral the sites of the spinel lattice, accompanied by a reverse transfer of Fe^{3+} ions from the octahedral to the tetrahedral sites. Consequently, the composite powder has a structural formula close to $(Fe_{0.98}Co_{0.02})[Co_{0.98}Fe_{1.02}]O_4$, which remains far from that assumed for seed powder, $(Fe_{0.86}Co_{0.14})[Co_{0.86}Fe_{1.14}]O_4$, where parentheses and square brackets correspond to the A and B spinel sites, respectively. This cation migration phenomenon, mediated by a prolonged in-time heating, was already reported on nickel–zinc spinel ferrite NPs produced by the polyol process and annealed in air at different temperatures.[27] In that work, the authors showed that the tetrahedral and octahedral sites of the spinel structure in the as-prepared particles

Table 2. Main structural and microstructural characteristics of the produced powders as inferred from XRD analysis. Typically, the cell parameter a, the average size coherent diffraction domain size $<L_{XRD}>$, and the weight content of each constituting phase are indicated. Additionally, the average total particle diameter $<D_{TEM}>$ inferred from TEM observation is given.

Sample	XRD analysis								TEM analysis
	Spinel phase				Rock-salt phase				
	a [Å] ±0.005	$<L_{XRD}>$ [nm] ±1	wt [%] ±10	$<\varepsilon>$ [%]	a [Å] ±0.005	$<L_{XRD}>$ [nm] ±1	wt [%] ±10	$<\varepsilon>$ [%]	$<D_{TEM}>$ [nm] ±0.5
CFO	8.403	10	100	0.04	–	–	–	–	9.3
CFO-CO	8.410	11	60	0.03	4.260	5	40	0.06	12.4

Table 3. Refined Mössbauer parameters from the spectra recorded at 300 and 77 K on the *CFO* and *CFO-CO* powders, using a least square fitting method and assuming Lorentzian line profile (the isomer shifts were referred to that of α-Fe at 300 K).

	$T = 300$ K			$T = 77$ K			
	$\langle\delta\rangle$ [mm s^{-1}] ±0.01	$\langle 2\varepsilon\rangle$ [mm s^{-1}] ±0.01	$\langle B_h\rangle$ [T] ±0.5	δ [mm s^{-1}] ±0.01	2ε [mm s^{-1}] ±0.01	B_h [T] ±0.5	Ratio (at %) ±2
CFO	0.33	0.03	43.5	0.51	+0.07	53.7	43
	–	–	–	0.38	−0.01	50.8	57
CFO-CO	0.33	0.02	44.9	0.52	+0.01	53.8	34
	–	–	–	0.40	−0.02	51.3	66

were all occupied by three types of cations, Ni^{2+}, Zn^{2+}, and Fe^{3+}, but after annealing, the concentration of tetrahedrally Ni^{2+} and octahedrally Zn^{2+} coordinated cations decreased to zero like in the expected thermodynamically stable structure.[27]

So, these results underline the limit of XRD in the discrimination between the two spinel structures and also highlight the fact that the F component in the composite powder must exhibit a larger magnetocrystalline anisotropy energy constant than in the seed one.

To complete our XRD structural analysis of the produced powders, the refined average lattice micro-deformation parameter $\langle\varepsilon\rangle$ and crystal size $\langle L_{XRD}\rangle$ of each phase were also determined by MAUD refinements, and are summarized in Table 1. The obtained values suggest that both spinel and rock-salt phases consist of almost strain-free crystals of some nanometers in size. Transmission electron microscopy (TEM) was finally performed and micrographs of different magnitudes were collected on seed and composite powders and compared (**Figure 3**a,b). The particle population of both samples appears uniform in size, with an average diameter $\langle D_{TEM}\rangle$ of 9.3 and 12.4 nm, respectively (Figure SI-2, Supporting Information). As a first approximation, if we consider the *CFO* cores as hard solid spheres covered by a *CO* dense, continuous and uniform coating, the latter value can be consistent with the increase of the initial seed core diameter by ≈3 nm, in agreement with the formation of a core–shell arrangement between the *CFO* and *CO* phases; the thickness of the latter being of about 1.5 nm (Figure 3c,d). High-resolution TEM observations (HRTEM) and fast Fourier transform (FFT) analyses showed that the seed powder results from well-defined, almost isotropic in shape, single crystals of about 9 nm in size. Their FFT pattern is related to a spinel structure observed along the [–110] direction,

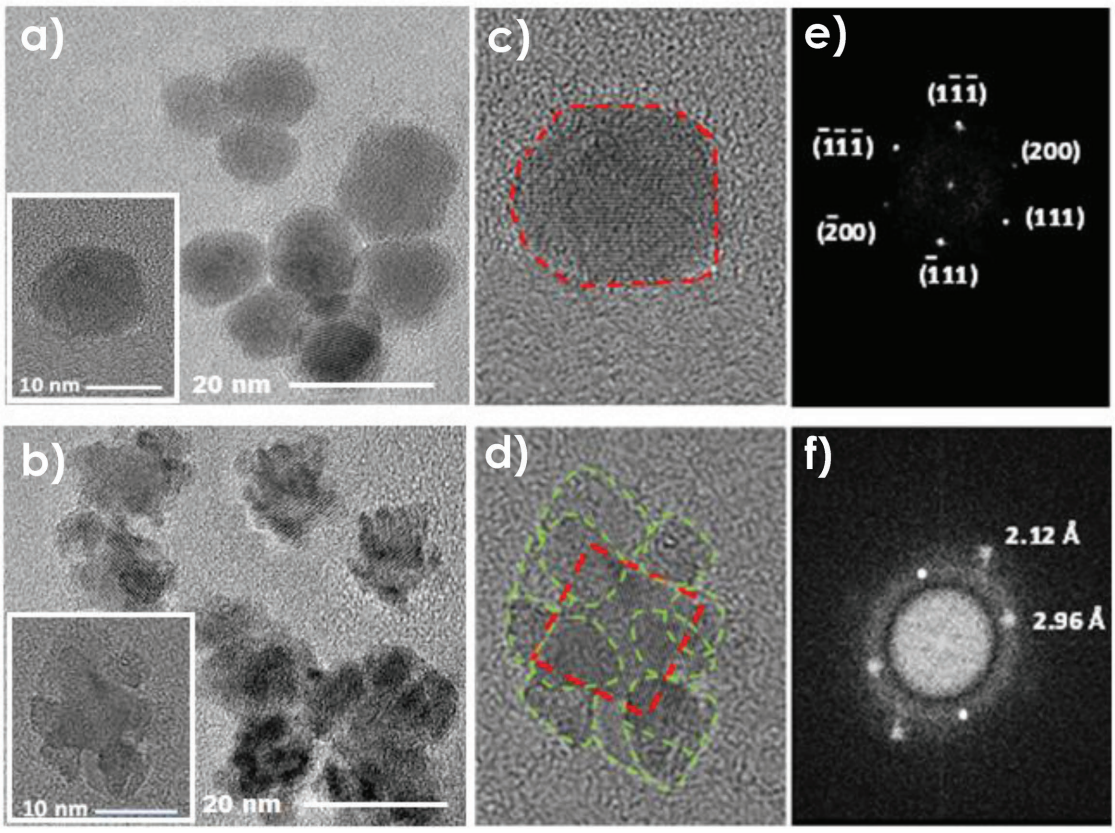

Figure 3. TEM micrographs of an assembly of a) *CFO* core and b) *CFO-CO* core–shell NPs. c,d) are HRTEM images of one representative particle of each system. Red and green dashed lines are added as eye-guides to delimit the *CFO* and *CO* outline nanocrystals. e,f) Corresponding FFT patterns.

the measured reticular distances being consistent with the {111} and the harmonic of the {400} planes (ICDD n°98-010-9044), namely 4.846 and 2.098 Å, respectively. In contrast, the composite powder appears to be constituted by almost isotropic NPs with a more complex architecture. Indeed, their structure differs between their inner core and their outer shell, suggesting a core@shell like structure. The inner core corresponds to the spinel cobalt ferrite crystal with a mean size of about 9 nm, surrounded by less than 4 nm sized rock-salt CoO satellites, with epitaxial relationships. The two phases have the same orientation within each single aggregate, without any evidence of structural defects such as dislocations, stacking faults, or surface amorphous region. These observations confirmed the high crystalline quality of the produced composite particles and pointed out their textured polycrystalline arrangement. The FFT patterns recorded on selected HRTEM images (Figure 3e,f) can be easily indexed by the highlighted 2.96 and 2.12 Å distances. The former matches with the (220) spinel planes and the harmonic of the (220) rock-salt ones, while the latter fits with the spinel (400) and the rock-salt (200) planes. By selecting the first diffraction spot (2.96 Å), the inverse FFT allowed us to obtain a lattice image of a representative core–shell particle (Figure SI-3, Supporting Information) and confirmed the epitaxial quality of the arrangement of the involved oxide phases.

To correlate TEM results to XRF and XRD measurements, we calculated the *CO* weight content from the following geometrical model and we compared the obtained value to those inferred from the previous chemical and structural analyses. For that, we considered each composite particle as a solid *CFO* sphere with a diameter *D* equal to 9.3 nm (that of the seed particles) surrounded by a continuous and dense *CO* shell with a thickness *d* equal to 1.5 nm (as estimated from the statistical analysis of the TEM images of an assembly of composite particles). The obtained *CO* content as calculated by Equation (1), where ρ_{CoO} and $\rho_{CoFe_2O_4}$ represent the density of bulk CoO and $CoFe_2O_4$, 6.44 and 5.20 g cm^{-3}, respectively, was estimated to be about 54%.

$$\text{CoO wt\%} = 100 \times \frac{d \times \rho_{CoO}}{\frac{D \times \rho_{CoFe_2O_4}}{6} + d \times \rho_{CoO}} \quad (1)$$

This value is higher than those inferred from XRF (42 wt%) and XRD (40 wt%) analyses. This discrepancy is mainly due to the fact that our composite particles are not exact core–shell particles, but they are much more like core-satellite ones, with a core and satellite size of about 9–10 nm and 3–4 nm, respectively. Nevertheless, a rapid calculation of the number *n* of *CO* satellites on a single *CFO* core, using XRD and XRF results in Equation (2), leads to an estimation of the coverage ratio, *r*, of *CO* on *CFO* surface (Equation (3)).

$$n = \frac{0.40 \times D^3 \times \rho_{CoFe_2O_4}}{0.60 \times d^3 \times \rho_{CoO}} \quad (2)$$

$$r = \frac{n \times d^2}{D^2} \quad (3)$$

With a *n* value of about 10 and a *r* slightly higher than 100% are obtained, meaning that the satellites remain relatively close to each other over the *CFO* surface, like an almost continuous layer. This feature is important for EB evidence. For these reasons, we continue describing our system as a core–shell like one.

2.2. Magnetic Properties

The variation of the DC magnetic susceptibility as a function of temperature χ(T) and the variation of the magnetization as a function of magnetic field *M*(H) were measured on both seed and composite powders. In practice, the as-produced powders were dispersed in diamagnetic alumina (4.23 wt%) and slightly compacted in a plastic sampling tube, before the measurements, in order to prevent NP's movement during the experiments and to reduce their mutual dipolar interactions. All the collected data were corrected from the diamagnetic contribution and expressed per gram of particles.

As expected, both *CFO* and *CFO-CO* powders exhibit a superparamagnetic behavior. Interestingly, their blocking temperature values are different. The average T_B value of the former is lower than that of the latter. Determined as the position of the maximum of the ZFC-χ(T) branch, T_B is about 250 K for *CFO* particles while it exceeds 350 K for their composite counterparts (**Figure 4**). These values suggest an increase of the effective magnetic anisotropy constant of the F phase in CFO-CO, as a consequence of i) the spinel magnetocrystalline anisotropy energy constant increase (the spinel local structure change) and ii) the exchange interaction implementation by EB coupling (the epitaxial growth of the rock-salt lattice around the spinel one).

In the same order of ideas, whereas the room temperature *M*(T) curve of *CFO* powder does not exhibit hysteresis feature, that of the *CFO-CO* one does it (**Figure 5**). For this sample, a weak but non-zero coercivity and remanence were observed: $\mu_0 H_C$ = 38 mT and M_r = 7.8 Am^2 kg^{-1}, respectively, for a saturation magnetization M_s of 62.5 Am^2 kg^{-1}. EB feature is confirmed by the evidence of a net loop shift along the

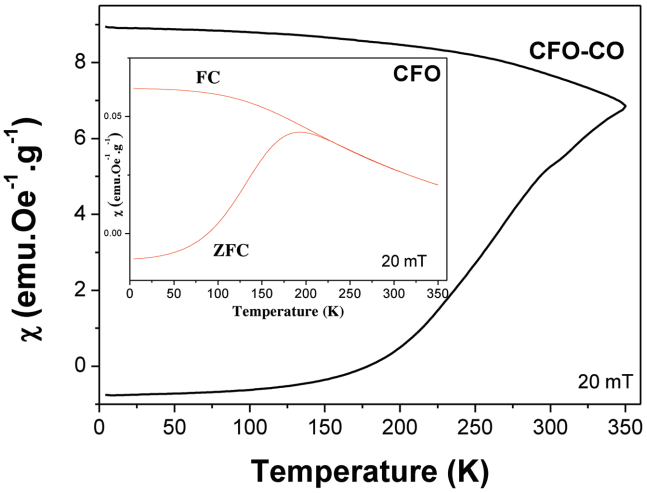

Figure 4. Thermal variation of the ZFC–FC susceptibility of the composite powder, measured under an applied magnetic field of 20 mT, compared to that of the seed powder (inset).

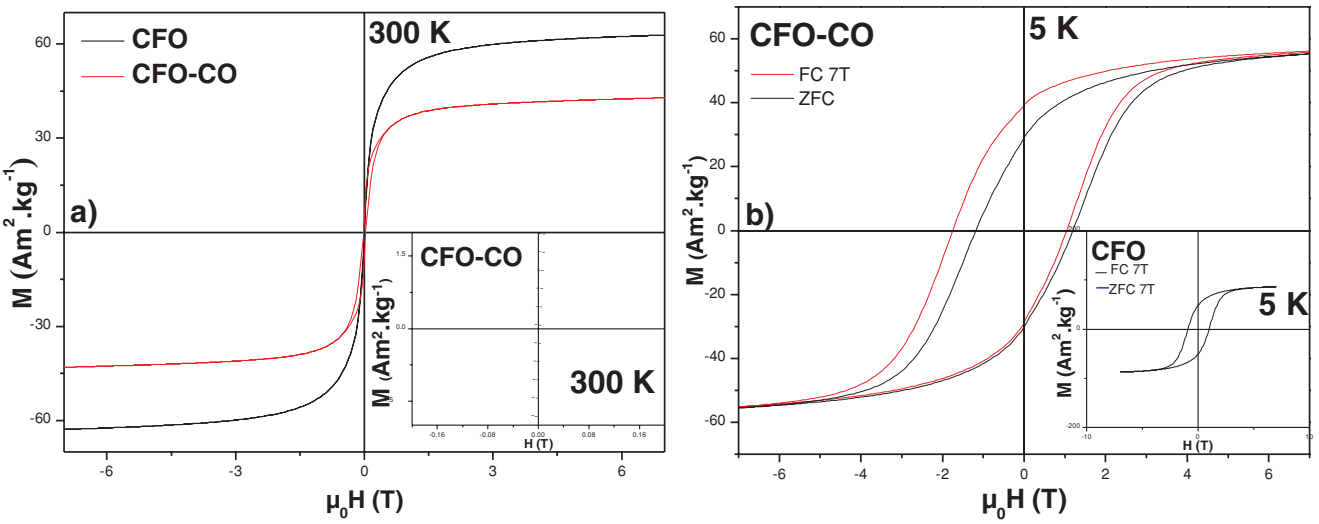

Figure 5. Variation of the magnetization as a function of the magnetic field, recorded on *CFO* seed and *CFO-CO* composite powders at 300 K (left) and 5 K (right). On the left side, the inset depicts a zoom of the *CFO-CO* powder 300 K-*M*(H) plot, while in the right side it depicts the *CFO* powder 5 K-*M*(H) plot.

magnetic field axis in the recorded *M*(H) curve at 5 K, after cooling from room temperature under an applied magnetic field of 7 T. The plot is clearly shifted toward negative magnetic field values (Figure 5), leading to an exchange field $\mu_0 H_E$ of 365 mT. This shift is accompanied by a loop broadening, since a coercive field $\mu_0 H_C$ of 1395 mT was measured on the FC-loop, by comparison to the 1190 mT in the ZFC and 947 mT in both the FC and ZFC loops of the seed powder (**Table 4**). The two phases in our system (CoO and $CoFe_2O_4$) have high anisotropy. The magnetocrystalline bulk anisotropy of the $CoFe_2O_4$ is $>3 \times 10^7$ erg cm^{-3},[36] but it is not well determined for the CoO phase and there is a wide dispersion of this value for CoO in the relevant litterature. The shift observed here indicates that the effective anisotropy of the CoO phase is larger than that of $CoFe_2O_4$ phase. In this case, the AF phase exerts a pinning action on the magnetization of the F phase giving rise to a sizeable loop shift.

Note that measured value of $\mu_0 H_E$ = 365 mT on the composite particles is significantly higher than the best values recently reported on oxide-based granular composites called "giant exchange-bias" systems, like $NiFe_2O_4$-CoO,[37] $SrFe_{12}O_{19}$@CoO,[21] $CoFe_2O_4$@Co_3O_4,[24] and others[38–44] summarized in Table SI-1 in the Supporting Information. These results are very promising and make our engineered *CFO-CO* composites particularly valuable as starting powder for the production of exchange-biased oxide-based consolidates.

Another indication of EB onset in the *CFO-CO* particles can be found in the increase of their M_r/M_s ratio, as inferred from their 5 K-FC-*M*(H) data, by comparison to that of bare *CFO* particle. A value of 0.7 is measured versus 0.5, consisting of the switching from cubic to uniaxial anisotropy, as usually reported for exchange-biased systems.[11] The last important and converging result concerns the saturation magnetization of the *CFO-CO* composite powder. Designating the saturation magnetization of *CO* shell in the *CFO-CO* core–shell particles, that of *CFO* core and their related *CFO-CO* composite counterparts as M_{sat}(shell), M_{sat}(core), and M_{sat}(core-shell), respectively, the cobalt ferrite weight content, *x*, in the composite particles can be deduced from the following equation:

$$x.M_{sat}(\text{shell}) + (1-x).M_{sat}(\text{core}) = M_{sat}(\text{core}-\text{shell}) \quad (4)$$

In the present case, M_{sat}(shell) is assumed to be equal to 0 Am^2 kg^{-1}, M_{sat}(core) is taken as equal to that of seed particles, namely 86.9 Am^2 kg^{-1}, and M_{sat}(core–shell) is equal to 55.5 Am^2 kg^{-1}. A cobalt ferrite weight content of 60 wt% was thus estimated, in good agreement with that determined by XRF, XRD, and TEM analyses.

3. Conclusions

$CoFe_2O_4$-CoO composite nanopowders were successfully produced by seed mediated growth in polyol. A giant EB ($\mu_0 H_E$ = 365 mT), at 5 K with a magnetic field cooling of 7T

Table 4. Main magnetic characteristics of the produced composite and seed powders deduced from their hysteresis loops recorded at 5 K in the FC (cooling field of +7T) and ZFC modes.

	ZFC			FC			
	M_s(5 K,0T) [Am^2 kg^{-1}] ± 0.5	M_r(5 K,0T) [Am^2 kg^{-1}] ± 0.5	$\mu_0 H_C$(5 K,0T) [mT] ± 2	M_S(5 K,7T) [Am^2 kg^{-1}] ± 0.5	M_r(5 K,7T) [Am^2 kg^{-1}] ± 0.5	$\mu_0 H_C$(5 K,7T) [mT] ± 2	$\mu_0 H_E$ (5 K,7T) [mT] ± 2
CFO	86.9	48.0	946	86.9	48.0	947	0
CFO-CO	55.3	30.0	1190	55.7	39.1	1395	365

field, accompanied by an amelioration of the $\mu_0 H_C$, was measured for this system. The produced composites consist of quite isotropic $CoFe_2O_4$ single crystals surrounded by rock-salt CoO satellites, forming an almost continuous coating, within a perfect epitaxial lattice relationship. A net evolution of the ferrite structure from a stoichiometric and mixed spinel cation arrangement, to a still stoichiometric, but an exact inverse spinel cation distribution, was observed during the particle preparation. Due to EB onset, magnetic properties of the contrasted core–shell particles were heightened, and the blocking temperature of the ferrite phase becomes higher than 350 K under an applied magnetic field of 20 mT in the composite particles, while it does not exceed 250 K in pristine cobalt ferrite ones, bearing the technological limits of superparamagnetism.

4. Experimental Section

Chemicals: Tetrahydrated cobalt (II) and anhydrous iron (II) acetate salts were purchased from SIGMA-ALDRICH and MERCK, respectively. Diethylene glycol (*DEG*) and triethylene glycol (*TEG*) were purchased from ACROS. All were used without any further purification.

Composite Particle Preparation: CFO particles were produced by the well-known polyol method and were synthesized by dissolving 12.5 mmol cobalt (II) acetate salt and 25.0 mmol iron (II) acetate salt into 125 mL of *TEG* and heating under reflux and mechanical stirring for 3 h. The suspension was allowed to cool down with continued stirring and the obtained solids were recuperated by centrifugation and washed with ethanol. They were then dried overnight at 50 °C. Then, for synthesizing the core–shell NPs, a mass of the as-produced *CFO* (1.32 g) was dispersed in a fresh solution of tetrahydrated cobalt (II) acetate salt (3.12 g) in *DEG* (250 mL), and used to serve as seeds around which the *CO* shell may grow. The mass of *CFO* seeds and cobalt acetate precursors were chosen assuming a final *CFO* and *CO* weight content of 60 and 40 wt%, respectively. The mixture was heated up to ebullition (200 °C) and maintained under reflux and mechanical stirring for 18 h, leading to the production of the desired *CFO-CO* core–shell particles. The recuperation of the composite particles was identical to the previous one: centrifugation, washing, and finally drying at 50 °C overnight.

Particle Characterization: The chemical composition of the produced powders was obtained using a MINIPAL4 XRF spectrometer equipped with a rhodium X-ray tube operating at 30 kV and 87 µA. Their crystalline structure was checked by XRD using a Panalytical X'pert Pro diffractometer, working in the Bragg–Brentano reflection geometry and equipped with a multichannel X'celerator detector and a cobalt X-ray tube operating at 40 kV and 40 mA radiation. To determine more precisely the structure of the spinel phase in the prepared samples, ^{57}Fe Mössbauer spectrometry was carried out at 300 and 77 K in a transmission geometry using a 57Co/Rh γ-ray source mounted on a conventional constant acceleration vibrating electromagnetic transducer. The powdered samples consist of 5 mg Fe cm^{-2} while the isomer shift values are quoted to that of α-Fe standard at 300 K.

Detailed microstructural analysis was performed on suspensions of *CFO* and *CFO-CO* powders, sonicated for few minutes in ethanol before deposition of a few drops on copper-coated carbon grids. TEM and HRTEM experiments were performed on a JEOL JEM 2100 Plus and a JEOL JEM 2010 UHR microscopes, both operating at 200 kV. The images were collected with a 4008 × 2672 pixel CCD camera (Gatan Orius SC1000).

The magnetic properties of the as-produced NPs were determined using a Quantum Design MPMS-5S SQUID magnetometer. To do so, the thermal variation of the magnetic susceptibility of each sample was measured between 5 and 330 K within both FC and ZFC conditions for an applied DC magnetic field of 200 Oe. Then the ZFC isothermal variation of their magnetization as a function of the magnetic field was measured between +70 and −70 kOe at 5 and 300 K, dispersing first the NPs in a diamagnetic alumina (Kaiser, 99.9%) matrix (4.8 wt%) to limit the effect of dipolar interactions on their whole magnetic behavior. At the end, the temperature dependence of the high field (70 kOe) spontaneous magnetization was measured at different temperatures. All the data were expressed per gram of powder and corrected from the diamagnetic contribution of alumina and the sampling plastic tube.

Supporting Information

Supporting Information is available from the Wiley Online Library and from the author.

Acknowledgements

All the authors contributed equally to this work. This work was supported by French Ministry of Research and National Centre for Scientific Research. The authors gratefully acknowledge ANR (Agence Nationale de la Recherche) and CGI (Commissariat à l'Investissement d'Avenir) for their financial support of this work through the IDEX SPC (ANR 11 IDEX 05 02) and LABEX SEAM (ANR 11 LABX 086) grants. The authors also thank Dr. Sophie Nowak (Paris Diderot University) and Dr. David Hrabovsky (Sorbonne University) for their technical assistance in XRD and SQUID measurements and analysis, respectively.

Conflict of Interest

The authors declare no conflict of interest.

Keywords

giant exchange-bias, interface effect, Mössbauer spectrometry, oxide-based core@shell nanoparticles, polyol process, superparamagnetism

Received: July 6, 2018
Revised: August 1, 2018
Published online: August 23, 2018

[1] W. H. Meiklejohn, C. P. Bean, *Phys. Rev.* **1956**, *102*, 1413.
[2] C. Tsang, T. Lin, S. MacDonald, M. Pinarbasi, N. Robertson, H. Santini, M. Doerner, T. Reith, L. Vo, T. Diola, P. Arnett, *IEEE Trans. Magn.* **1997**, *33*, 2866.
[3] K. Stoev, F. Liu, Y. Chen, X. Dang, P. Luo, J. Chen, J. Wang, K. Kung, M. Lederman, M. Re, G. Choe, J. N. Zhou, M. Yu, *J. Appl. Phys.* **2003**, *93*, 6552.
[4] S. Giri, M. Patra, S. Majumdar, *J. Phys.: Condens. Matter* **2011**, *23*, 073201.
[5] R. H. Koch, G. Grinstein, G. A. Keefe, Y. Lu, P. L. Trouilloud, W. J. Gallagher, S. S. P. Parkin, *Phys. Rev. Lett.* **2000**, *84*, 5419.
[6] R. W. Cross, Y. K. Kim, J. O. Oti, S. E. Russek, *Appl. Phys. Lett.* **1996**, *69*, 3935.
[7] J. Sort, J. Nogués, X. Amils, S. Suriñach, J. S. Muñoz, M. D. Baró, *Appl. Phys. Lett.* **1999**, *75*, 3177.
[8] J. Sort, S. Suriñach, J. S. Muñoz, M. D. Baró, J. Nogués, G. Chouteau, V. Skumryev, G. C. Hadjipanayis, *Phys. Rev. B* **2002**, *65*, 174420.
[9] J. Eisenmenger, I. K. Schuller, *Nat. Mater.* **2003**, *2*, 437.
[10] V. Skumryev, S. Stoyanov, Y. Zhang, G. Hadjipanayis, D. Givord, J. Nogués, *Nature* **2003**, *423*, 850.
[11] J. Noguès, I. K. Schuller, *J. Magn. Magn. Mater.* **1999**, *192*, 203.

[12] G. Salazar-Alvarez, J. Sort, S. Suriñach, M. D. Baró, J. Nogués, *J. Am. Chem. Soc.* **2007**, *129*, 9102.
[13] T. Gaudisson, L. Ourry, H. Hammoud, S. Nowak, N. Menguy, N. Yaacoub, J.-M. Grenèche, F. Mammeri, S. Ammar, *J. Nanopart. Res.* **2014**, *16*, 2359.
[14] J. Nogués, J. Sort, V. Langlais, S. Doppiu, B. Dieny, J. S. Munoz, S. Surinach, M. D. Baró, S. Stoyanov, Y. Zhang, *J. Nanotechnol.* **2005**, *2*, 23.
[15] B. Martínez, X. Obradors, L. Balcells, A. Rouanet, C. Monty, *Phys. Rev. Lett.* **1998**, *80*, 181.
[16] N. Domingo, D. Fiorani, A. M. Testa, C. Binns, S. Baker, J. Tejada, *J. Phys. D: Appl. Phys.* **2008**, *41*, 134009.
[17] Y. Guo, L. Shi, S. Zhou, J. Zhao, C. Wang, W. Liu, S. Wei, *J. Phys. D: Appl. Phys.* **2013**, *46*, 175302.
[18] D. Niebieskikwiat, M. B. Salamon, *Phys. Rev. B* **2005**, *72*, 174422.
[19] M. Patra, S. Majumdar, S. Giri, *J. Phys.: Condens. Matter* **2010**, *22*, 116001.
[20] M. H. Yu, P. Sujatha Devi, L. H. Lewis, P. Oouma, J. B. Parise, R. J. Gambino, *Mater. Sci. Eng., B* **2003**, *103B*, 162.
[21] X. S. Liu, B. X. Gu, W. Zhong, H. Y. Jiang, Y. W. Du, *Appl. Phys. A: Mater. Sci. Process.* **2003**, *77*, 673.
[22] M. P. Buron, M. Gougeon, A. Rousset, *Key Eng. Mater.* **1997**, *132–136*, 1420.
[23] M. Artus, S. Ammar, L. Sicard, J.-Y. Piquemal, F. Herbst, M.-J. Vaulay, F. Fiévet, V. Richard, *Chem. Mater.* **2008**, *20*, 4861.
[24] F. L. Zan, Y. Q. Ma, Q. Ma, Y. F. Xu, Z. X. Dai, G. H. Zheng, *J. Alloys Compd.* **2013**, *581*, 263.
[25] M. Artus, L. B. Tahar, F. Herbst, L. Smiri, F. Villain, N. Yaacoub, J.-M. Grenèche, S. Ammar, F. Fiévet, *J. Phys.: Condens. Matter* **2011**, *23*, 506001.
[26] S. Chkoundali, S. Ammar, N. Jouini, F. Fiévet, P. Molinié, M. Danot, F. Villain, J.-M. Grenèche, *J. Phys.: Condens. Matter* **2004**, *16*, 4357.
[27] Z. Beji, L. S. Smiri, N. Yaacoub, J.-M. Grenèche, N. Menguy, S. Ammar, F. Fiévet, *Chem. Mater.* **2010**, *22*, 1350.
[28] L. Lutterotti, S. Matthies, H. R. Wenk, *IUCr CPD Newsl.* **1999**, *21*, 14.
[29] R. J. Hill, *Am. Mineral.* **1984**, *69*, 937.
[30] T. Yamanaka, *Phys. Chem. Miner.* **1986**, *13*, 227.
[31] I. K. Sedler, A. Feenstra, T. Peters, *Eur. J. Mineral.* **1994**, *6*, 873.
[32] (a) P. Poix, *C. R. Acad. Sci. Paris C* **1969**, *268*, 1139; (b) R. J. Hill, J. R. Craig, G. V. Gibbs, *Phys. Chem. Miner.* **1979**, *4*, 317; (c) H. S. O'Neill, A. Navrotsky, *Am. Mineral.* **1983**, *68*, 181.
[33] G. A. Petitt, D. W. Forester, *Phys. Rev. B* **1971**, *4*, 3912.
[34] N. Moumen, P. Veillet, M. P. Pileni, *J. Magn. Magn. Mater.* **1995**, *149*, 67.
[35] J.-M. Grenèche, M. Miglierini, *Mössbauer Spectroscopy in Materials Science*, NATO Science Series, Springer, Dordrecht **1999**, pp. 243–256.
[36] J. Tracy, D. Weiss, D. Dinega, M. Bawendi, *Phys. Rev. B* **2005**, *72*, 64404.
[37] R. Mohan, M. P. Ghosh, S. Mukherjee, *Mater. Res. Express* **2018**, *5*, 035029.
[38] Q. Xing, Z. Han, S. Zhao, *Mater. Lett.* **2017**, *188*, 103.
[39] S. P. Pati, A. Roychowdhury, S. Kumar, D. Das, *J. Appl. Phys.* **2013**, *113*, 17D708.
[40] D. De, Ò. Iglesias, S. Majumdar, S. Giri, *Phys. Rev. B* **2016**, *94*, 184410.
[41] Z. Swiatkowska-Warkocka, K. Kawaguchi, H. Wang, Y. Katou, N. Koshizaki, *Nanoscale Res. Lett.* **2011**, *6*, 226.
[42] J. Sort, V. Langlais, S. Doppiu, B. Dieny, S. Suriñach, J. S. Muñoz, M. D. Baró, C. Laurent, J. Nogués, *Nanotechnol.* **2004**, *15*, S211.
[43] M. Kaur, J. S. McCloy, Y. Qiang, *J. Appl. Phys.* **2013**, *113*, 17D715.
[44] G. Franceschin, T. Gaudisson, N. Menguy, B. C. Dodrill, N. Yaacoub, J.-M. Grenèche, R. Valenzuela, S. Ammar, *Part. Part. Syst. Charact.* **2018**, 1800104.

